FINAL REPORT FOR THE PERIOD

10/1/93 - 9/30/97

to

OFFICE OF NAVAL RESEARCH

Grant No: N00014-94-I-0086

PREDICTION OF HYDROGEN ENTRY AND PERMEATION IN METALS AND ALLOYS

H. W. Pickering

Department of Materials Science and Engineering
The Pennsylvania State University
University Park, PA 16802

REPORT DOCUMENTATION PAGE

Form Approved
OMB No. 0704-0188

1. AGENCY USE ONLY (Leave blank)	2. REPORT DATE	3. REPORT TYPE AND DATES COVERED
	October 1997	Final 10/1/93 to 9/30/97

4. TITLE AND SUBTITLE
Prediction of Hydrogen Entry and Permeation in Metals and Alloys

5. FUNDING NUMBERS
N00014-94-I-0086

6. AUTHOR(S)
Howard W. Pickering

7. PERFORMING ORGANIZATION NAME(S) AND ADDRESS(ES)
The Pennsylvania State University
Department of Materials Science and Engineering
326 Steidle Building
University Park, PA 16802

8. PERFORMING ORGANIZATION REPORT NUMBER

9. SPONSORING/MONITORING AGENCY NAME(S) AND ADDRESS(ES)
Scientific Officer
Materials Division Code: 1131M
Office of Naval Research
Arlington, VA 22217-5000
ATTN: A. John Sedriks,

10. SPONSORING/MONITORING AGENCY REPORT NUMBER

11. SUPPLEMENTARY NOTES

12a. DISTRIBUTION/AVAILABILITY STATEMENT
Approved for public release; distribution is unlimited.

12b. DISTRIBUTION CODE

13. ABSTRACT *(Maximum 200 words)*

The objectives of this research were to understand the mechanism of hydrogen entry into metals and to search for and evaluate various remedial measures to control this process and the subsequent hydrogen embrittlement. Several parallel approaches were pursued to achieve these objectives. A brief description is given in the report on each of these following tasks: Twenty-two research and review papers were published or submitted to journals which describe the progress on these tasks.

14. SUBJECT TERMS
KEY WORDS: hydrogen absorption, hydrogen embrittlement, chloride ions, benzotriazole, underpotential deposition, environmental cracking, sensitized stainless steel, anodic protection, pits and crevices, IR drop.

15. NUMBER OF PAGES

16. PRICE CODE

17. SECURITY CLASSIFICATION OF REPORT	18. SECURITY CLASSIFICATION OF THIS PAGE	19. SECURITY CLASSIFICATION OF ABSTRACT	20. LIMITATION OF ABSTRACT

RESEARCH GOALS

The goal of this research project was to achieve the following objectives: (i) identify and evaluate the effects of the key factors that influence the process of hydrogen entry into metals particularly steels and lead to their subsequent embrittlement under various service conditions, and (ii) search for and develop remedial measures. Three parallel approaches were pursued simultaneously, i.e. (a) Identification of the conditions which lead to the unexpected generation of hydrogen within crevices, pits and localized corrosion grooves around grain boundaries or non-metallic inclusions. (b) Measurements of the rates of hydrogen permeation through metals e.g. iron and some steels, and (iv) evaluation of some additives as inhibitors for the absorption of hydrogen in iron.

SUMMARY OF RESULTS

The progress achieved on the project is summarized in the following points:

1. Conditions for hydrogen absorption within cavities and grain boundary grooves

We have investigated the conditions which lead to the generation of hydrogen within surface cavities. Such cavities exist at the junctions of metals with other materials or at the surface intersections of inclusions in metals, or form during service, e.g., cracks which are initiated under open circuit or cathodic/anodic protection situations. The results showed that the aspect ratio (depth/width) is a most important property of the system. This aspect ratio is independent of the actual depth of a cavity. Hence, a very shallow crack and a very deep crack may have the same aspect ratio but have different widths. This result is readily obtained based on a modeling analysis in one of our earlier ONR sponsored research publications (Ateya and Pickering, 1975). Consequently, a shallow crack could, in principle, have the same IR drop as a deep crack since the magnitude of the IR is a function of the aspect ratio rather than simply of the crack depth. The

consequences of this independence of aspect ratio and cavity depth has led to a working hypothesis on how stabilization of pit growth following passive film breakdown may occur (1). The concept is equally powerful for the analysis of crack formation and stabilization during both cathodic and anodic polarization where either hydrogen absorption or metal dissolution may be responsible for the cracking event. A discussion of the aspect ratio in the context of potential distribution within localized corrosion processes is presented in our publications including those listed for this reporting period (2).

2. Crevicing Paths

An analysis was also performed on the various localized corrosion paths (3). Fig. 1 illustrates the various combinations (paths) of changes in acidity and electrode potential, E, which are encountered in crevice corrosion on a Pourbaix diagram. The arrows refer to the direction of change of E and pH, starting from the external passive surface of the crevice towards its actively dissolving interior. Paths 1 and 3 illustrate limiting cases. Path 1 is a large increase in acidity and no change in E (no IR voltage). Path 3 is a large shift of E in the negative direction (large IR voltage) with no change in acidity. Path 1 describes a hypothetical limiting case in which the increase in acidity destroys passivity under potentials in the passive region. It is strictly applicable only when the electrolyte has infinite conductivity, such that the flow of the current within the crevice electrolyte causes no IR voltage. This path cannot represent real systems. In reality, the crevice electrolyte has a finite resistivity, which can be rather high in view of its geometry, particularly in the presence of solid or gaseous corrosion products which constrict the current path and lead to very large IR voltages. In such systems, the increase in acidity within the crevice is necessarily associated with an IR voltage and associated shift of the electrode potential, E(x), in the negative direction in promoting crevice corrosion, as path 2 illustrates.

Path 3 can be attained by continuous mixing of the crevice electrolyte with the bulk solution, by buffering the solution, or if the bulk electrolyte is at the equilibrium pH of the hydrolysis of the metal ions, i.e., ~pH 4 for Fe and pH 2 for Ni. Except in the case of mixing, this potential shift will be accompanied by anion accumulation, e.g., chloride if chloride ions are present in the

solution, and other changes in solution composition even though there is no acidification. A major finding on the project was that in the total absence of concentration changes (convective mixing case), path 3 (i.e., IR voltage by itself) was shown to produce stable crevice corrosion (4), confirming earlier results on the project for constant pH conditions using a buffer. This result experimentally refuted the earlier published positions by some researchers that IR voltages were merely a consequence of the crevice corrosion process.

Path 4, like path 2, represents a case where potential drops are accompanied by pH and other composition changes within the crevice but for path 4 the pH increases unlike path 2. Path 4 is encountered in strongly acidic bulk electrolytes whereas path 2 is encountered in higher pH bulk solutions. Thus, whereas crevice corrosion for path 2 involves acidification, path 4 involves deacidification. For both paths 2 and 4, chloride accumulation occurs if the bulk solution contains chloride ions. Chloride ion accumulation is also expected for path 3 except when convective mixing occurs during crevice corrosion as shown elsewhere (4).

Paths 3 and 4 illustrate situations in which the IR potential drop promotes crevice corrosion but there are no significant or favorable pH changes. Rather, the change in pH in path 4 tends to lower the stability of an ongoing crevice corrosion process as shown elsewhere (4). Either a buffer solution or convective mixing maintains the pH within the crevice close to that of the bulk solution (path 3). For the case of a constant pH produced by a buffer, the polarization curve of the metal in the crevice electrolyte does not change from that of the bulk electrolyte except to the extent caused by changes in concentration of species other than hydrogen ions. In the case of convective mixing, the concentrations of all species in the crevice electrolyte approximates those of the bulk electrolyte throughout the experiment so that the polarization curve of the crevice electrolyte remains close to that of the bulk electrolyte. In this case, the bulk solution polarization curve can be used to predict the characteristics of the crevice corrosion process as shown (4). Since in path 3 and also in path 4 where any compositional changes that occur are largely unfavorable for promoting crevice corrosion, it is clearly the IR voltage that stabilizes the crevice corrosion process. It does so by

shifting the electrode potential, E(x), at locations within the crevice to less noble values and into the active peak of the polarization curve where the IR > $\Delta\phi^*$ criterion is met.

For polarization curves with active/passive transitions, crevice corrosion begins immediately if the IR > $\Delta\phi^*$ condition is met at time zero, i.e., there is no induction period. Conversely, an induction period exists prior to the onset of crevice corrosion when the IR > $\Delta\phi^*$ condition is not initially met, if the solution composition changes in such a way so as to increase I or R, and/or decrease $\Delta\phi^*$. This is expected for path 2 where acidification increases the size of the active peak but not for path 4. For example, for iron or corrosion-resistant alloys in neutral or alkaline solutions, induction periods typically exist prior to the onset of crevice corrosion. It remains to be determined whether or not the induction period ends when the changes in the polarization curve, as caused by acidification, are sufficient to enable the above IR criterion to be met. In the presence of chloride ions in the bulk electrolyte, the IR voltage (the potential field) causes them and other anions to migrate into and accumulate within the crevice (in the absence of convective mixing). As in the case of acidification, this may lead to progressive increases in the size of the active peak. As such, the role of Cl^- ion would be consistent with the scenario that the induction period ends as IR $\geq \Delta\phi^*$ is approached (since I increases and $\Delta\phi^*$ decreases). These effects have been recently discussed (4) and are currently under study.

3. Distribution of anodic and cathodic reaction sites during environmentally assisted cracking.

We have analyzed the effects of charge and mass transport limitations on the distribution of cathodic and anodic reactions on the flanks of environmentally assisted cracks (5). Under conditions of cathodic protection of the metal surface, it is shown that the presence of recesses or cracks leads to significant changes in the potential and ionic concentrations at various distances into the cavity. Consequently, the rate of the hydrogen evolution reaction decreases with increasing distance into the cavity. For base metals and alloys, e.g., Fe or Ni, metal dissolution occurs with progressively increasing rates at increasing distance into the crack. The variations of these cathodic and anodic current distributions with distance within the crack (or with the time of cracking)

depends on the dimension of the opening of the crack, *a*, the diffusivity of the hydrogen ion, D_H, and, hence, the conductivity of the electrolyte, and the polarization at the external surface of the metal, $\eta(0)$. Analysis of the migration-diffusion problem leads to the development of a characteristic depth given by

$$Z=\left[\frac{FD_H+C_H^o a}{i_o H}\exp\frac{(\beta\eta(0))}{b}\right]^{1/2} \text{ cm}$$

where $c^o_{H^+}$ is the acid concentration, and β and i_0 are the charge transfer coefficient and the exchange current density of the hydrogen evolution reaction, respectively. Z has a strong effect on the behavior of the system.

Figure 2 illustrates the geometry of the crack, while Figures 3 - 5 illustrate the distributions of potentials and currents within cracks of various opening dimension *a* and various values of Z. The figures also show the positions, within the crack, where iron dissolution starts to occur.

4. Chromium depletion

We have shown that the dissolution of the Cr-depleted zones around the grain boundaries of sensitized Type 430 stainless steel leads to the generation of subsurface grooves which grow and branch out within the substrate alloy which has normal chromium content. This establishes local conditions which lead to the generation of hydrogen within the grooves, and to subsequent hydrogen embrittlement (6-8). We observed subsurface grooves which are up to 50 fold wider than the width of the Cr-depleted zone in Type 430 stainless steel. We have also shown that hydrogen gas is being evolved within these grooves, even though their external surface is under conditions which prohibit such a reaction. Details of these investigations appear elsewhere (6-8).

Our focus on the generation of hydrogen gas within growing surface cavities and its subsequent absorption and embrittlement of the metal involved considerable amounts of mathematical modeling and experimental testing. Available results have been published and/or presented as reviews during the last few years (2, 5, 9, 10). Some of the consequences of these studies for metallic surfaces under cathodic polarization, impact on the need for an improved analytical characterization method for predicting (i) the success or failure of cathodic protection of recesses, (ii) the occurrence of active dissolution at the crack tip and adjacent crack flanks, and (iii) the distribution of hydrogen charging rate on the crack flanks.

5. Underpotential deposition and absorption of hydrogen (UPD)

The question of underpotential deposition of hydrogen is of particular concern to the problem of hydrogen embrittlement. For the case of hydrogen, underpotential deposition refers to hydrogen evolution (and hence absorption within the metal) at potentials more noble than the equilibrium potential of the hydrogen reaction by several tens of millivolts. We have obtained some preliminary results on the UPD of hydrogen on Pd where it was found that hydrogen entered and diffused through Pd while its surface was controlled at a more noble potential than the equilibrium potential of the hydrogen reaction. These measurements need to be continued and the results analyzed before testing the same phenomenon on iron.

6. The rate and distribution of the HER during shape evolution of an active crevice.

The shape evolution of an active crevice has been characterized from the onset to termination of the crevice corrosion process. The location of the HER within the crevice has been monitored by microscopic identification of (hydrogen) gas bubbles on the crevice surface. The bubbles and their growth were viewed in-situ through a transparent material (Plexiglas) that constitutes the other surface of the crevice. These studies are reported elsewhere (4,10-15).

7. Hydrogen embrittlement and stress corrosion in Ni containing ferritic stainless steels:

Work is underway to better understand the difference in environmentally induced cracking of ferritic stainless steels (AL 294®-29% Cr and 4% Mo) and ferritic stainless steels with minor Ni additions (AL 29-4-2®-29% Cr, 4% Mo and 2% Ni). The work which is currently being pursued involves electrochemical (polarization curves and potentiostatic) experiments on material which is stressed to better understand the interaction between the metal and solution which defines the susceptibility of the alloys to chloride SCC and HC. Surface and solution analysis will also be completed to determine what processes are occurring at the interface when these two alloys are exposed to an environment that is known to promote environmental crack propagation.

8. The role of chloride ion in modifying the rate of hydrogen absorption in iron:

We have shown that chloride ions reduce the overpotential for the HER on an iron surface in both acid and alkaline solutions at 23°C, and in turn reduce the hydrogen coverage and permeation of hydrogen (16). The effects on permeation are more pronounced in alkaline than in acid solutions, see Fig. 6. Permeation transients at constant electrode potential of the charging surface and subsequent surface (XPS) analyses of the uppermost atom layers of the hydrogen charged iron surface indicate (i) either a reversible or low coverage with Cl^- ions, (ii) a low hydrogen coverage which is not influenced significantly by Cl^- ion concentration at low overpotentials, and (iii) a marked effect of Cl^- ions on reducing the hydrogen coverage of the surface and the permeability in alkaline solutions at high cathodic polarizations.

9. Effects of BTA and BTA + Cu^{+2} as inhibitors for the hydrogen uptake by iron

BTA was shown to inhibit both the absorption of hydrogen within iron and the rate of hydrogen evolution (17). Figures 7 and 8 and Table 1 show some of these results. We have also obtained similar results on iron in nearly neutral medium, Fig. 9.

The addition of Cu^{2+} ions to BTA was shown in the literature to inhibit the general corrosion of cobalt. The inhibition was attributed to the formation of Cu^{+}/BTA film on the cobalt surface. We used the same idea to inhibit the hydrogen absorption on iron in acidic solution of 0.1N H_2SO_4 +

0.9N Na_2SO_4. The addition of Cu^{2+} to BTA also led to a decrease in rate of the HER. Figures 10 to 12 illustrate some of the results. These synergistic effects of BTA and Cu^{2+} ion are analyzed in detail elsewhere (18).

10. Kinetics of hydrogen absorption within iron using the IPZ model

We have long been concerned with the kinetics of hydrogen absorption within iron, which is the first step in the processes leading to hydrogen embrittlement and eventual failure of metals and alloys. A mechanistic (IPZ) model was presented earlier (19,20) which provides a method for calculating rate constants for the relevant processes in the absence of other adsorbing species. The model has been used in analyzing data of hydrogen absorption, e.g., in the presence of H_2S on an earlier ONR Grant (21), in the laboratory of R. E. White under conditions of electroplating iron with a protective layer of Zn (J. Electrochem. Soc., 143, 1871 (1996) and in the presence of thallium as a promoter of hydrogen entry into steel (J. Electrochem. Soc., 141, 1526 (1994)), and in the laboratory of B. E. Wilde under conditions of laser surface alloying to impede hydrogen entry into steel (Corros. Sci., 37, 607 (1995)). We are currently applying the model to measurements obtained in the presence of other adsorbing species, e.g., BTA.

11. STM of hydrogen adsorption on clean silicon

In this study some characterization of hydrogen adsorption and desorption from the gas phase on a clean, single crystal (100) silicon surface was achieved (22). At low coverages, hydrogen atoms resided on top of the dimerised Si atoms, and were imaged brightly. The hydrogen chemisorption induces buckling of dimers, indicating the strong bonding between Si and H atoms. With increasing coverage, both the (2 x 1) monohydride and (1 x 1) dihydride phases were formed. The former was imaged dark compared with the unreacted Si dimers, due to the reduction of the density of electronic states near the Fermi level. Surface etching was also observed. The extent of corrosion of the surface was modest in the monohydride phase, while during the formation of the dihydride phase, it became more significant. The behavior of hydrogen

desorption from the dihydride and monohydride phases was investigated as a function of annealing temperature. Our STM results support the mechanism that the desorbing H_2 molecules are formed by combination of two hydrogen atoms forming the dihydride phase. Upon annealing at elevated temperatures, Si overlayer stripes were formed by desorption of hydrogen from the etching products and the rearrangement of the Si atoms.

PUBLICATIONS AND REPORTS ON THE PROJECT

1. Yuan Xu, Minghua Wang and H. W. Pickering, "On Electric Field Induced Breakdown of Passive Films and IR Voltage Stabilization of Pitting Corrosion," J. Electrochem. Soc., 140, 3448-3457 (1993).

2. H. W. Pickering, "The Role of Electrode Potential Distribution in Corrosion Processes," J. Materials Sci. & Eng. A, A198, 213-223 (1995).

3. B. G. Ateya and H. W. Pickering, "The Interaction Between the IR Potential Drop and Composition Changes During the Activation and Propagation of Crevice Corrosion, "Proc. Corrosion 96, Reserch Topical Symposia, Part II - Crevice Corrosion: The Science and Its Control in Engineering Practice, NACE International, Houston, TX (1996), pp., 341-354.

4. M. Wang, H. W. Pickering, and Y. Xu, Potential Distribution, Shape Evolution and Modeling of Pit Growth for Ni in Sulfuric Acid, J. Electrochem. Soc., 142, 2986 - 2995 (1995).

5. B. G. Ateya and H. W. Pickering, "Distribution of Anodic and Cathodic Reaction Sites During Envrionmentally Assisted Cracking," Proc. Hydrogen Effects on Material Behavior, A. W. Thompson and N. R. Moody, eds., The Minerals Metals and Materials Soc., Warrendale, PA 15086 (1996), pp. 635-646; ibid., Corros. Sci., 37, 1443-1453 (1995).

6. W. Kelly, R. N. Iyer and H. W. Pickering, "Another Grain Boundary Corrosion Mechanism in Sensitized Stainless Steel," J. Electrochem Soc., 140, 3134-3140 (1993).

7. A. Sehgal, B. G. Ateya, and H. W. Pickering, "Hydrogen Evolution and Absorption Within Grain Boundary Grooves in Sensitized Stainless Steel Under Conditions of Anodic Polarization," J. Electrochem. Soc.,142, L198-L200 (1995).

8. A. Sehgal, B. G. Ateya, and H. W. Pickering, "Synergistic Effects of Chromium Depletion and Ohmic Potential Drop on the Susceptibility to Intergranular Corrosion and Hydrogen Embrittlement of Sensitized Stainless Steel," Acta Metallurgica et Materialia, 45, 3389-3399 (1997).

9. Brian DeForce and Howard Pickering, "A Clearer View of How Crevice Corrosion Occurs," JOM (J. Minerals, Metals & Materials Soc.), 22 (Sept. 1995).

10. Brian DeForce and Howard Pickering, "Recent Advances in Localized Corrosion," Proc. Annual Conference of the Egyptian Corrosion Society, 1-25 (Alexandria, Egypt, Sept. 27-28, 1995).

11. E. A. Nystrom, J. B. Lee, A. A. Sagüés and H. W. Pickering, "An Approach for Estimating Anodic Current Distributions in Crevice Corrosion from Potential Measurements," J. Electrochem. Soc., 141, 358 (1994).

12. E. A. Nystrom, H. W. Pickering, and A. A. Sagüés, "Current and Potential Distributions Inside Crevices in Rebar Steel and Other Metals," Proc. First Mexican Symposium on Metallic Corrosion, (Mérida, Yucatán, México, March 1994), pp. 1-11, L. Maldonado and M. Pech, Eds., ISBN 968-36-4811-8, UNAM Facultad de Quimica Press, Mexico D. F., (1995).

13. K. Cho and H. W. Pickering, "The IR Drop Mechanism of Crevice Corrosion," pp. 1277 - 1282 in The Proceedings of the International Conference for Korean Scientists and Engineers, volume of Materials and chemistry, ed., S. J. Kim, KOFST< Korea (1993).

14. Howard Pickering, Mingua Wang, Yuan Xu, "On the Effect of pH change and Ni^{2+} Ion Accumulation During Localized Corrosion in the Ni/1N H_2SO_4 System," Proc. Critical Factors in Localized Corrosion II Symp., P. M. Natishan, r. G. Kelly, G. s. Frankel and R. C. Newman, ed., Vol. 95-15, the Electrochemical Society Proceedings Series, Pennington, NJ (1996), pp. 151-161.

15. H. W. Pickering, "Compositional Changes Within Local Cells and Their Effects on the Stablility of the Local Cell Process," Extended Abstracts, Vol. 96-2; ibid, The Electrochemical Society Proceedings Series, Pennington, NJ (Oct. 6-11, 1996, San Antonio, TX); ibid, J. Electrochem. Soc., 144, 3364-2369 (1997).

16. A. M. Allam, B. G. Ateya, and H. W. Pickering, "Effect of Chloride Ions on the Absorption and Permeation of Hydrogen in Iron," Corrosion, 53, 284-289 (1997).

17. M. H. Abd Alhamid, B. G. Ateya, and H. W. Pickering, "Benzotriazole as an Inhibitior for the Hydrogen Uptake by Iron," Extended Abstracts, Vol. 96-2, The Electrochemical Society, Pennington, NJ (Oct. 6-11, 1996, San Antonio, TX), ibid., J. Electrochem. Soc., 144, L58 - L61(1997).

18. M. H. Abd Elhamid, B. G. Ateya, and H. W. Pickering, "Synergistic Effects of Benzotriazole and Copper Ions on the Absorption of Hydrogen Within Iron in Acid and Neutral Media," in preparation (1997).

19. R. Iyer, H. W. Pickering and M. Zamanzadeh, "Analysis of Hydrogen Evolution and Entry into Metals for the Discharge-Recombination Process", J. Electrochem. Soc., 136, 2463-2470 (1989).

20. R. N. Iyer and H. W. Pickering, "Mechanism and Kinetics of Electrochemical Hydrogen Entry and Degradation of Metallic Systems", Annual Review of Materials Science, Vol. 20, Annual Reviews, Inc., Palo Alto, Calif. (1990).

21. R. N. Iyer, I. Takeuchi, M. Zamanzadeh and H. W. Pickering, "Hydrogen Sulfide Effect on Hydrogen Entry into Iron - A Mechanistic Study", Corrosion, 46, 460 (1990).

22. X. Wang, H. Lu, T. Hashizume, H. W. Pickering, and T. Sakurai, "Atomic Hydrogen Chemisorption on Si (100) 2 x 1 Studied by FI-STM, Appl. Surface Sci., 67, 266-274 (1993).

23. TECHNICAL REPORT, Contract USN 00014-91-J-1189, February, 1993.

24. TECHNICAL REPORT, Contract USN 00014-91-J-1189, April, 1993.

25. TECHNICAL REPORT, Contract USN 00014-91-J-1189, May, 1993.

26. ANNUAL REPORT, Contract USN 00014-940I-0086, February, 1995.

27. ANNUAL REPORT, Contract USN 00014-94-I-0086, January, 1996.

28. ANNUAL REPORT, Contract USN 00014-96-I-0913, May, 1997.

Table I. Values of the steady-state permeation current, I, and the concentration of hydrogen in iron at the input surface, C°, at different concentrations of the BTA at a potential of -0.65 V (SCE).

[BTA], mM	I ($\mu A\ cm^2$)	C° ($mol\ cm^{-3}$)
0	2.17	4.7×10^{-8}
1	0.46	1.0×10^{-8}
10	0.24	5.0×10^{-9}
50	0.16	3.5×10^{-9}

FIGURE CAPTIONS

Figure 1. Illustration of the various paths of potential and pH change which lead to the generation of localized corrosion cells in iron-based systems.

Figure 2. Model of a crack in which the HER occurs on the outer surface (i_s) and on the crack walls. The bulk electrolyte is H^+ and Y^- and the outer (x = 0) surface conditions are E (0) and i_s.

Figure 3. Potential and HER current distributions within cracks of various depths for a value of the characteristic depth Z = 0.04 cm during cathodic polarization of the iron surface (see text).

Figure 4. Effect of the decrease in crack opening dimension *a* on the potential and current distributions for the conditions in Fig. 3.

Figure 5. Effect of the decrease in cathodic polarization at the outer surface, E(0), on the potential and current distributions for the conditions in Fig. 3.

Figure 6. Effect of Cl^- ion on the relation between i_∞ and E of the charging surface of the iron membrane.

Figure 7. Schematic illustration showing (a, top) the position of the iron membrane between the two electrolytic cells and (b, bottom) the boundary conditions imposed on the membrane by the two cells.

Figure 8. Steady-state permeation current (i_∞) vs. cathodic potential (-E at different BTA concentrations.

Figure 9. Hydrogen permeation transients obtained at different BTA concentrations, at a cathodic charging current of 1.25 mA cm^{-2}.

Figure 10. Hydrogen permeation transients obtained at a charging current density of 1.25 mA cm^{-2} for different charging solution compositions.

Figure 11. Hydrogen permeation transients obtained under open circuit potential for different charging solution compositions.

Figure 12. Steady state permeation current (i_∞) vs. cathodic potential (-E) for different charging solution compositions.

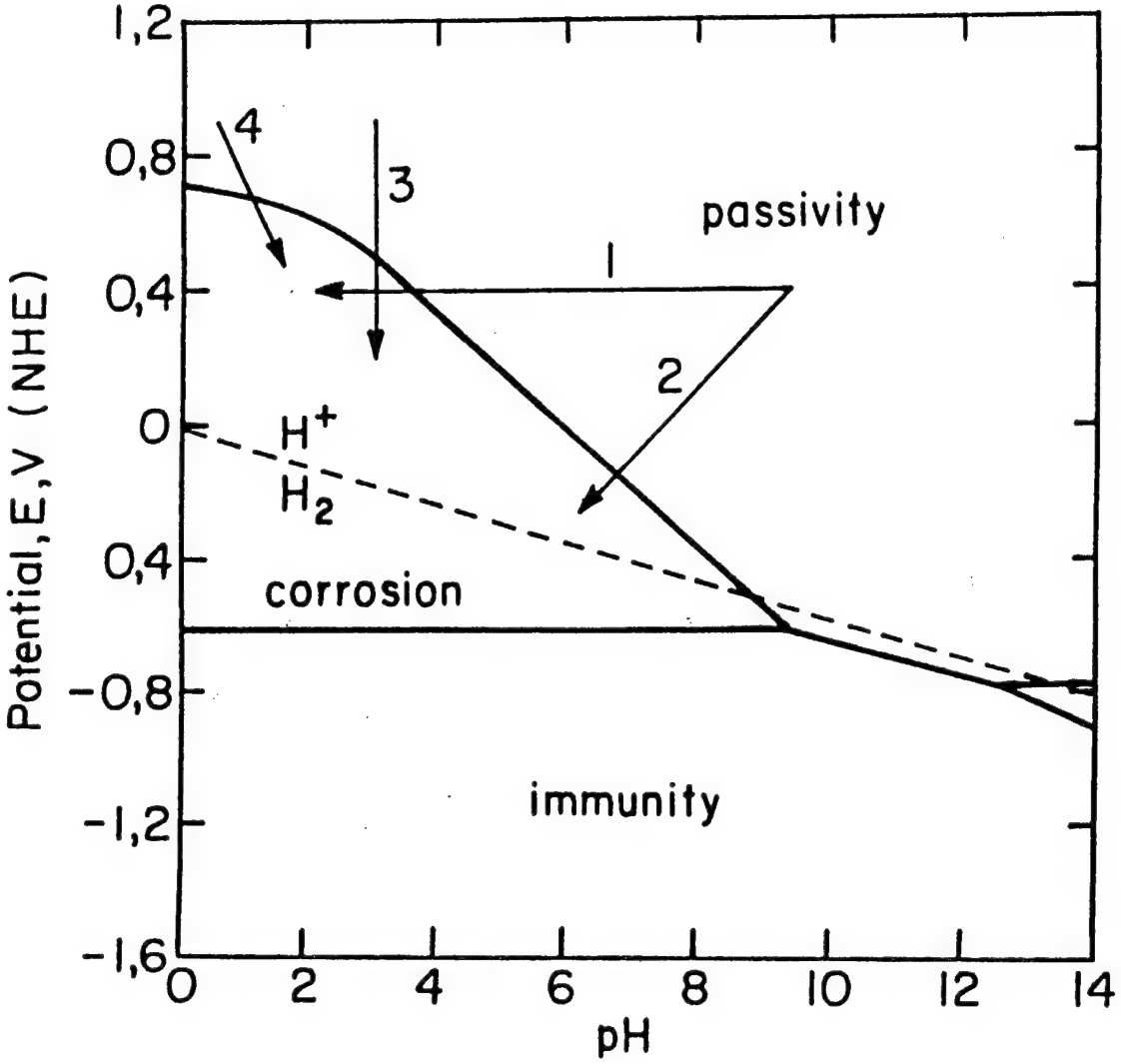

Figure 1 Illustration of the various paths of potential and pH change which lead to the generation of localized corrosion cells in iron-based systems.

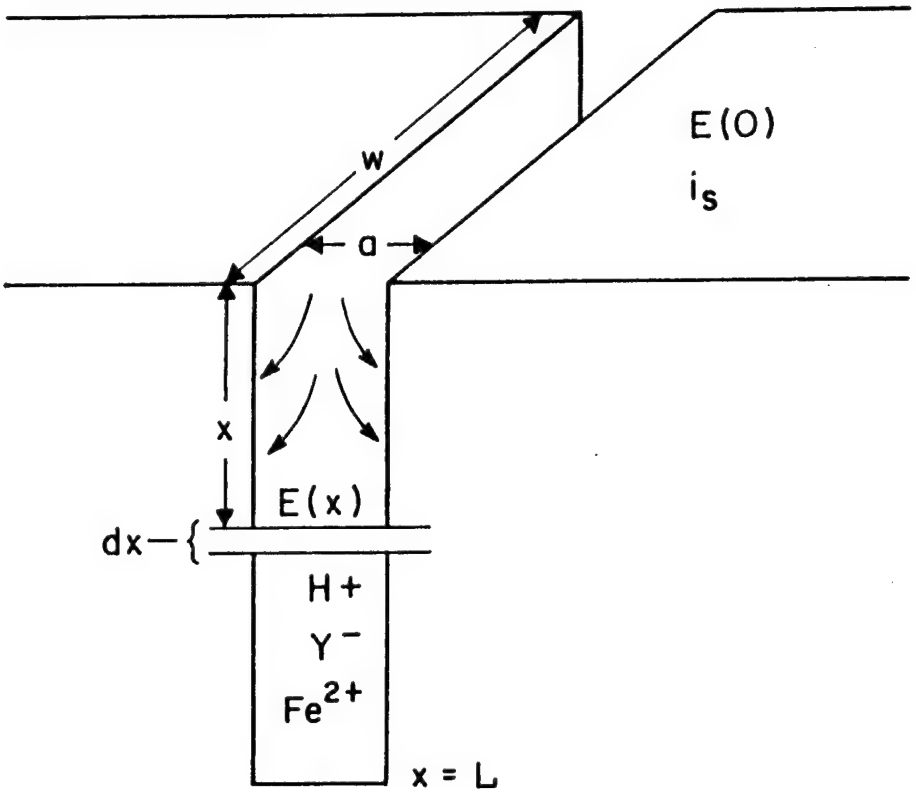

Figure 2 Model of a crack in which the HER occurs on the outer surface (i_s) and on the crack walls. The bulk electrolyte is H^+ and Y^- and the outer (x=0) surface conditions are E (0) and i_s.

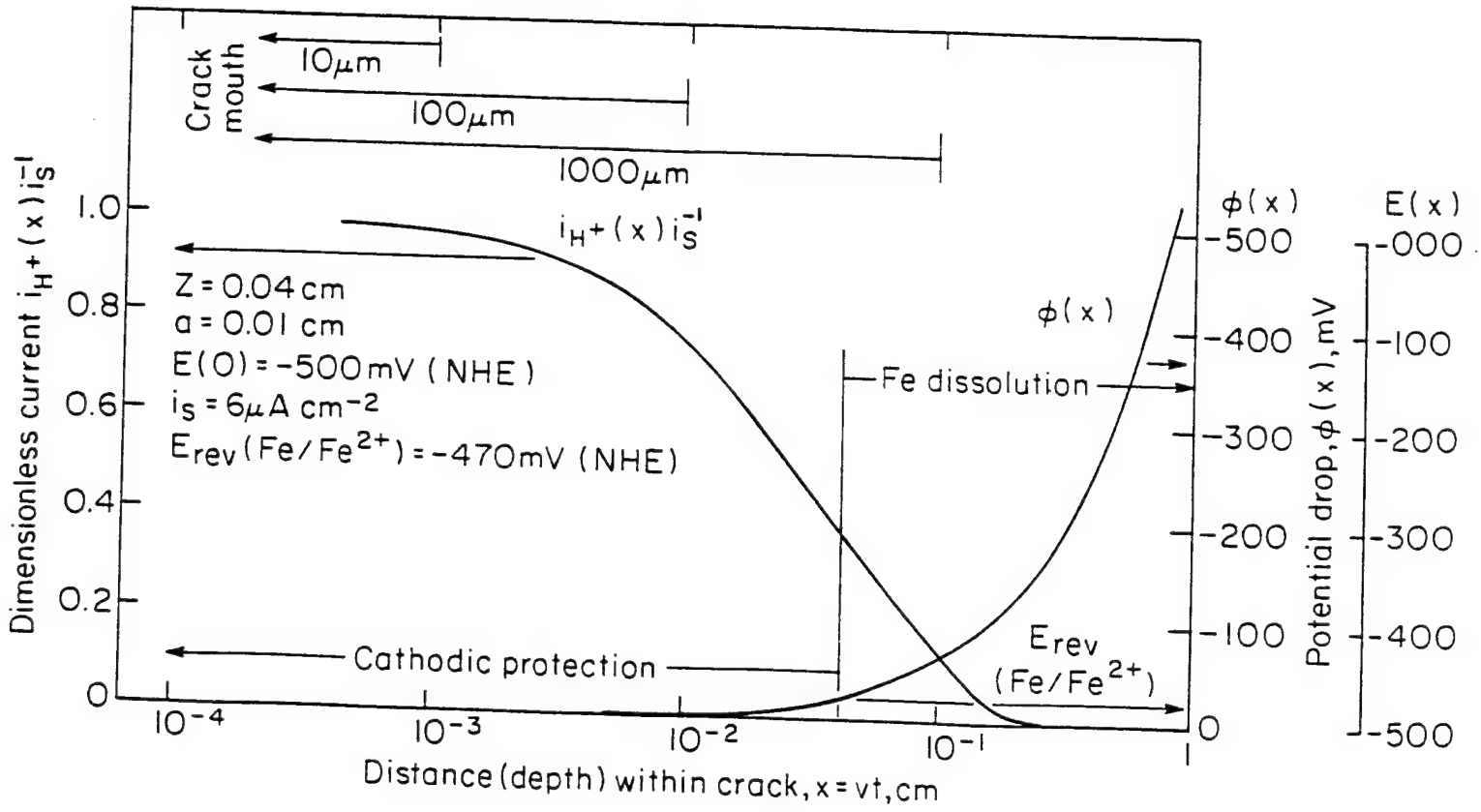

Figure 3 Potential and HER current distributions within cracks of various depths for a value of the characteristic depth Z=0.04 cm during cathodic polarization of the iron surface (see text).

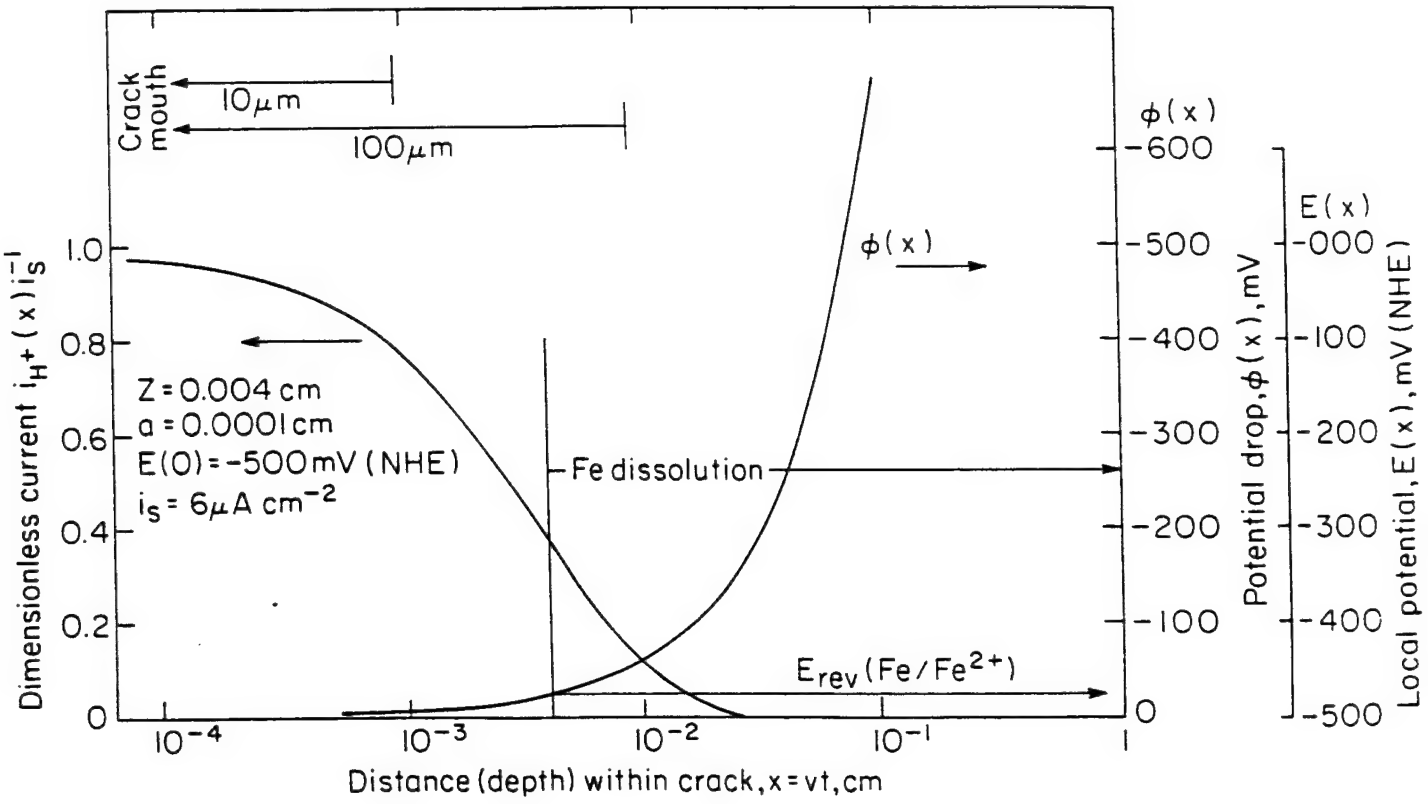

Figure 4 Effect of the decrease in crack opening dimension *a* on the potential and current distributions for the conditions in Fig. 3.

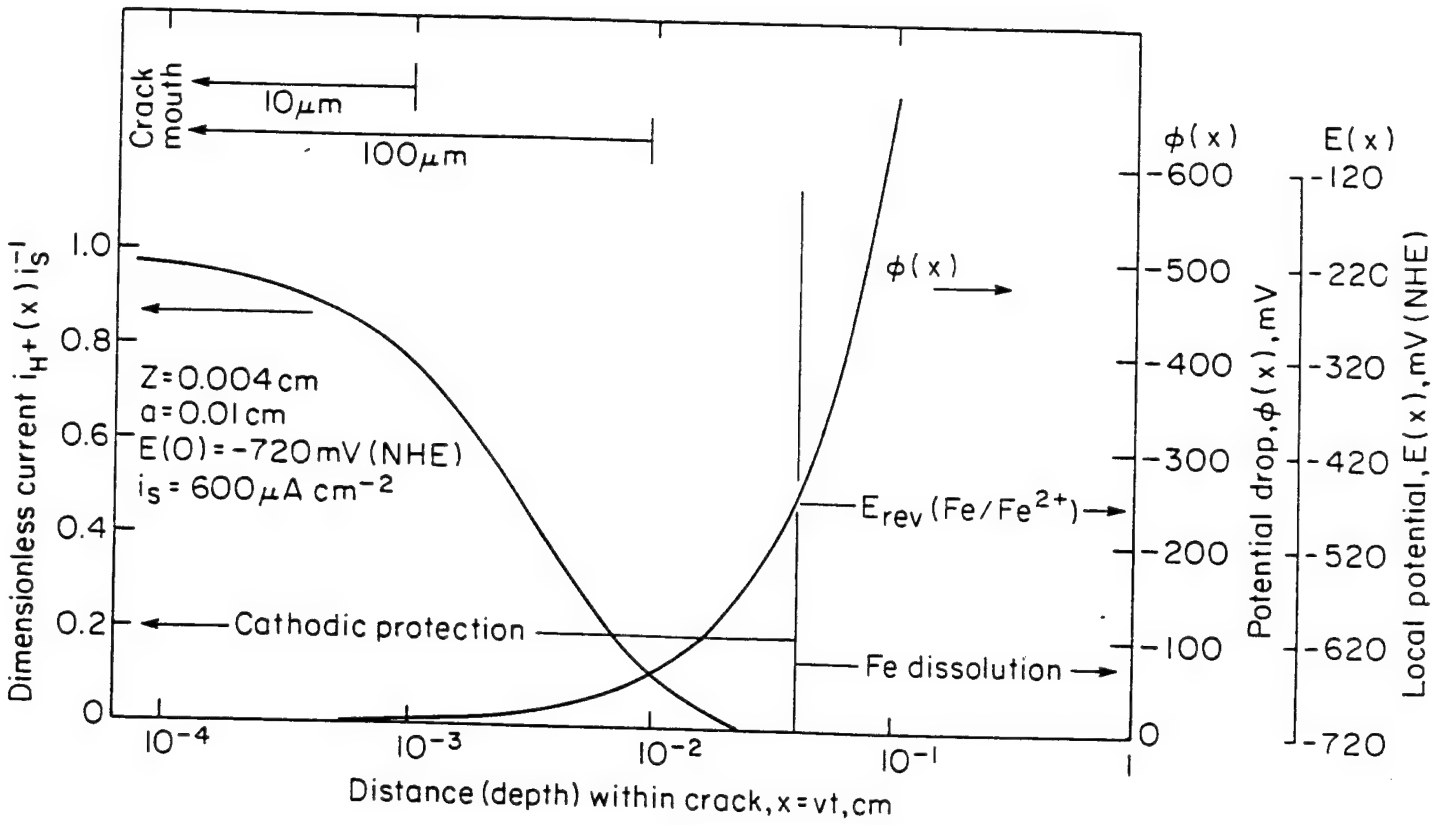

Figure 5. Effect of the decrease in cathodic polarization at the outer surface, E(0), on the potential and current distributions for the conditions in Fig. 3.

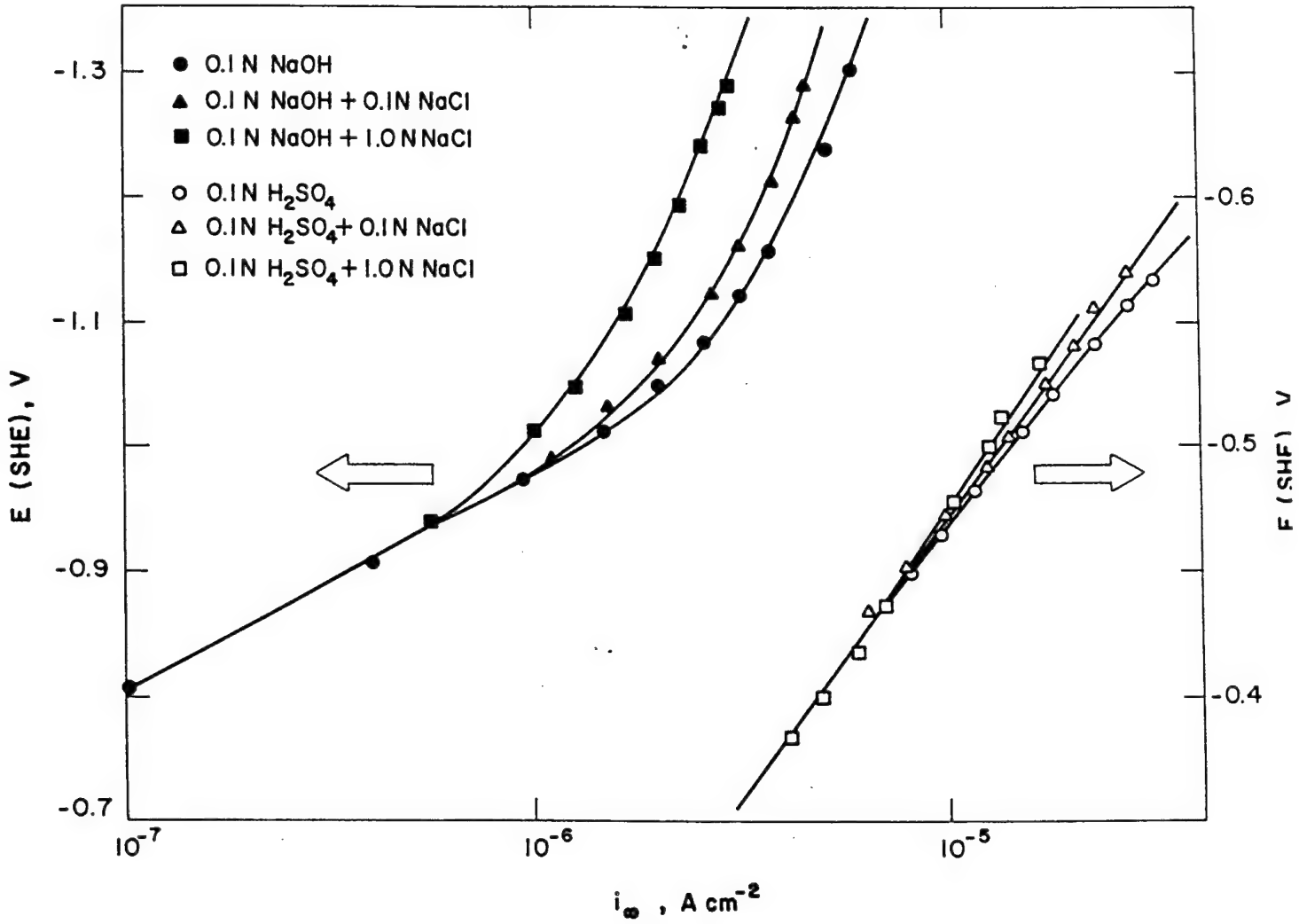

Figure 6 Effect of Cl^- ion on the relation between i_∞ and E of the charging surface of the iron membrane.

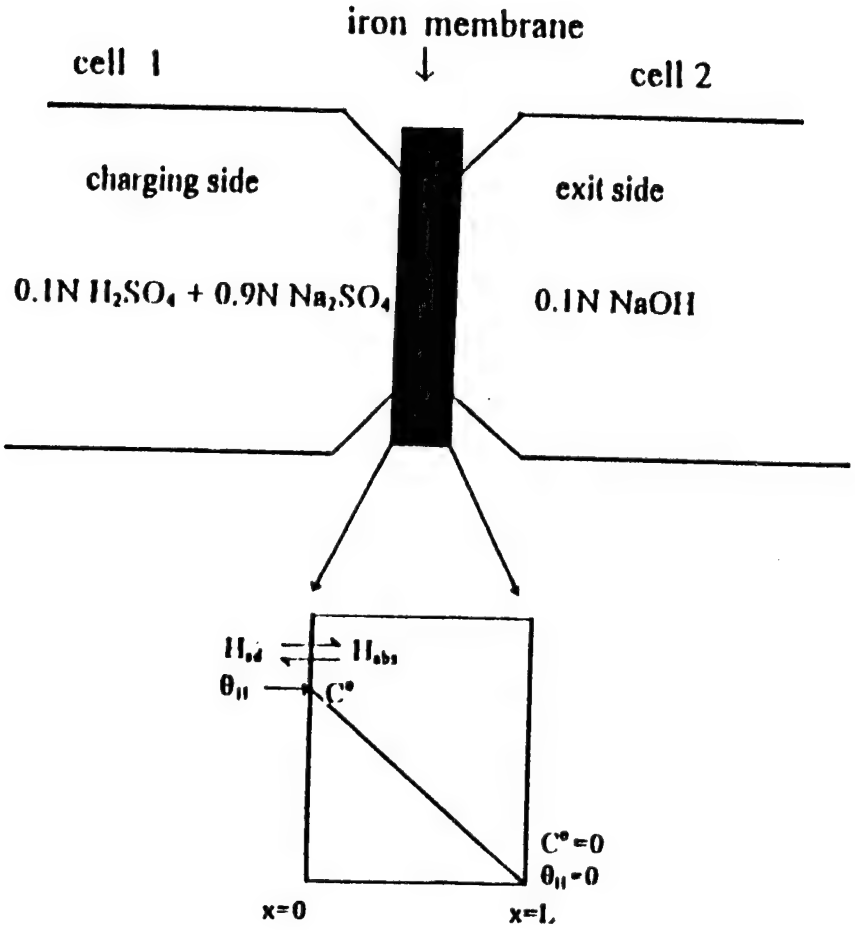

Figure 7 Schematic illustration showing (a,top) the position of the iron membrane between the two electrolytic cells and (b, bottom) the boundary conditions imposed on the membrane by the two cells.

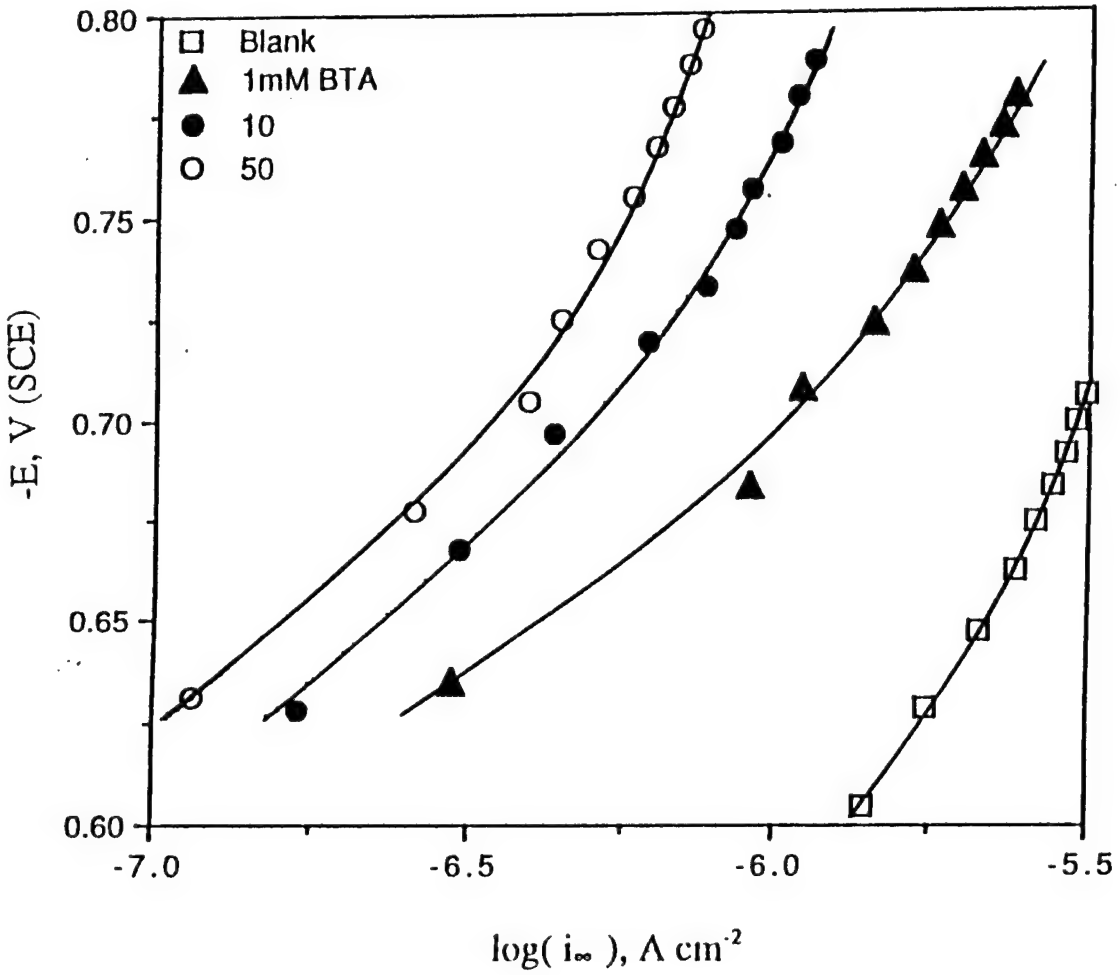

Figure 8 Steady-state permeation current (i_∞) vs. cathodic potential (-E) at different BTA concentrations.

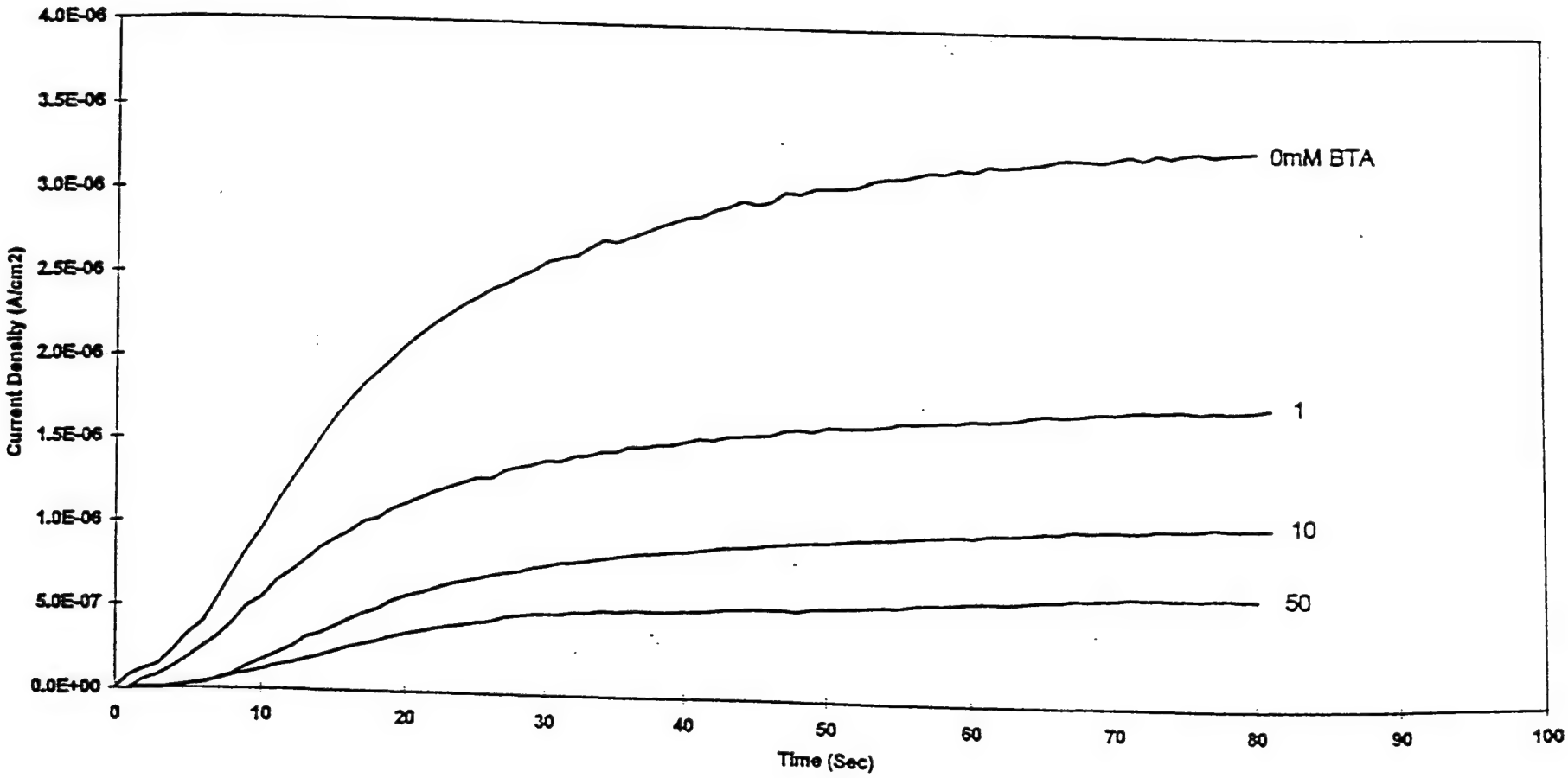

Figure 9 Hydrogen permeation transients obtained at different BTA concentrations, at a cathodic charging current of 1.25 mA cm^{-2}.

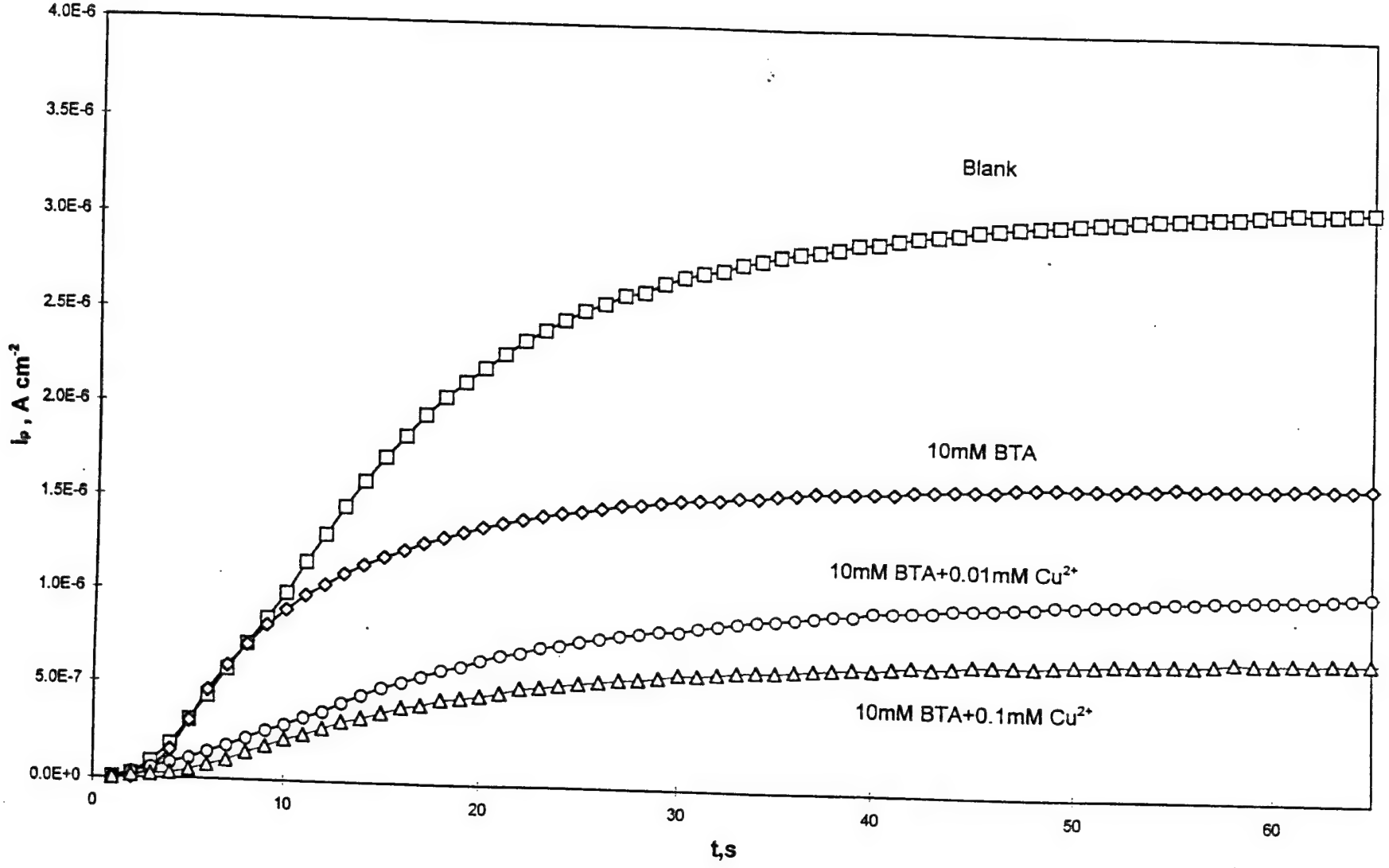

Figure 10 Hydrogen permeation transients obtained at a charging current density of 1.25 mA cm^{-2} for different charging solution compositions.

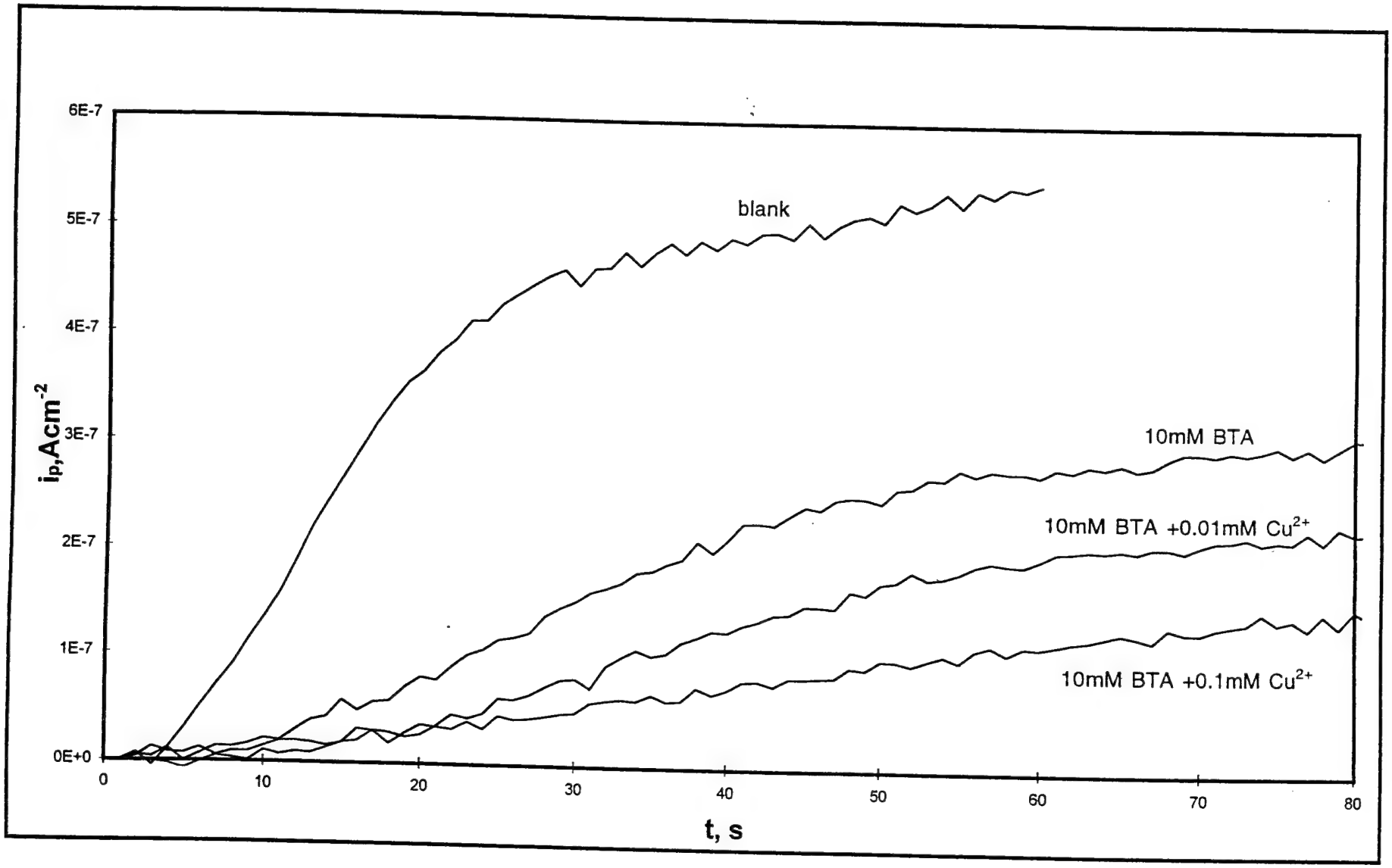

Figure 11 Hydrogen permeation transients obtained under open circuit potential for different charging solution compositions.

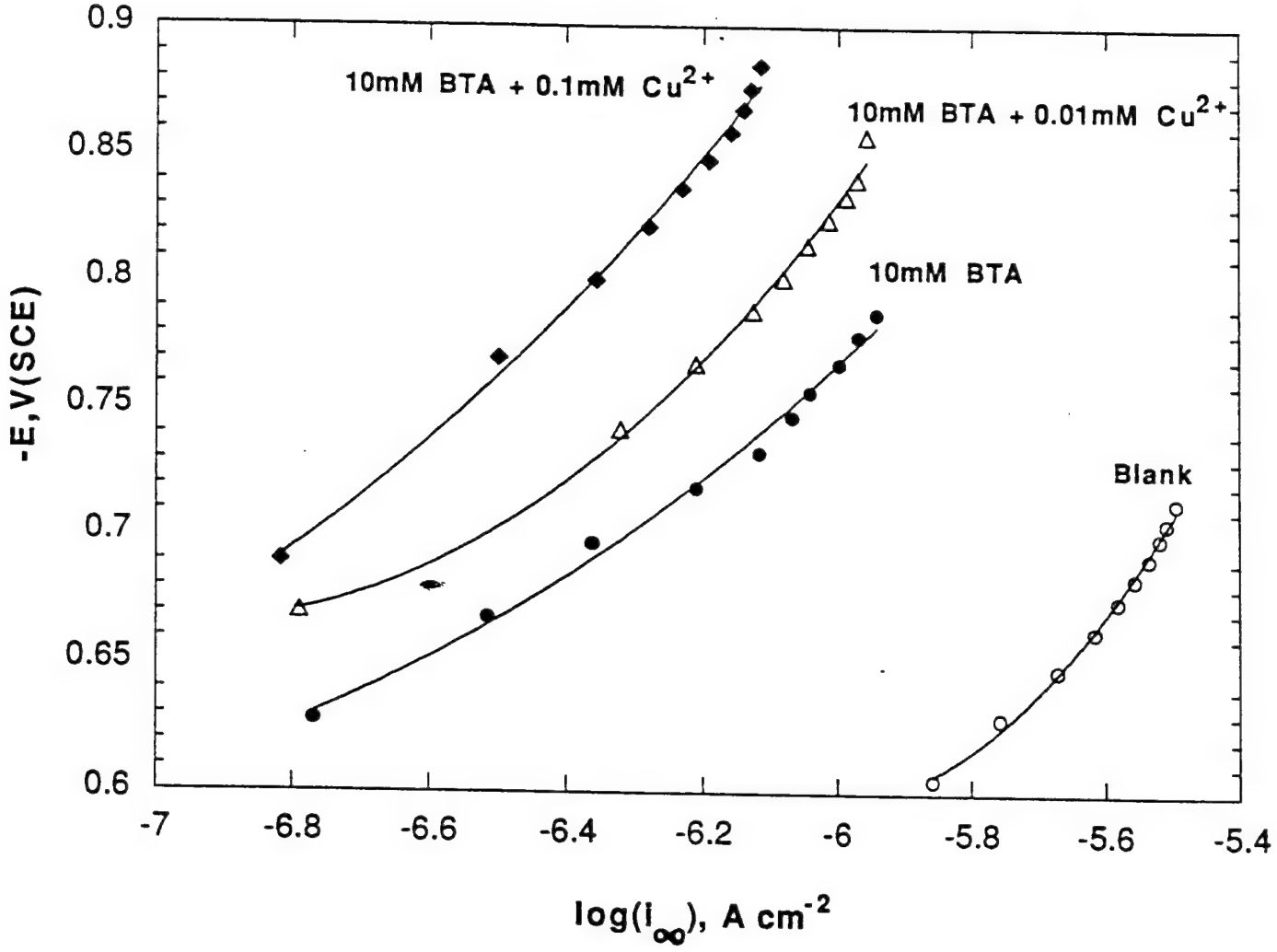

Figure 12 Steady state permeation current (i_∞) vs. cathodic potential (-E) for different charging solution compositions.

May 97

BASIC DISTRIBUTION LIST

Technical Reports and Publications

Organization	Copies
Defense Technical Information Center 8725 John J. Kingman Rd., Suite 0944 Ft. Belvoir, VA 22060-6218	2
Office of Naval Research 800 N. Quincy Street Arlington, VA 22217-5660 ATTN: Code 332	3
Naval Research Laboratory 4555 Overlook Ave., S.W. Washington, DC 20375 ATTN: Code 6000 Code 6300	1 1
Naval Surface Warfare Center Carderock Division Bldg. 60, Corrosion Branch 9500 McArthur Blvd. West Bethesda , MD 20817-5700 ATTN: Code 60	1
Naval Postgraduate School Monterey, CA 93940 ATTN: Mechanical Engineering Department	1
Naval Sea Systems Command Dept. of Navy 2531 Jefferson Davis Highway Arlington, VA 22242-5160 ATTN: Code 03M	1
Naval Air Warfare Center Aerospace Materials Division Code 4.3.4, Ms 3, Building 2188 Patuxent River, MD 20670-5304 ATTN: Code 4.3.4	1
Naval Facilities Engineering Service Center Port Hueneme, CA 94043 ATTN: Materials Div.	1
Naval Surface Warfare Center Carderock Division 9500 McArthur Blvd. West Bethesda, MD 20817-5700 ATTN: Library	1
Naval Underwater Warfare Center Newport, RI 02840 ATTN: Library	1
Naval Air Warfare Center Weapons Division China Lake, CA 93555-6001 ATTN: Library	1
NASA Lewis Research Center 21000 Brookpark Road Cleveland, OH 44135 ATTN: Library	1

Organization	Copies
Naval Command, Control and Ocean Surveilance Center R&D Division San Diego, CA 92152-5000 ATTN: Library	1
Office of the Assistant Commander HQ Marine Corps 2 Navy Annex Washington, DC 20380-1775 ATTN: Scientific Advisor	1
Army Research Office P.O. Box 12211 Research Triangle Park, NC 27709 ATTN: Metallurgy & Ceramics Program	1
Air Force Office of Scientific Research Building 410 Bolling Air Force Base Washington, DC 20332 ATTN: Electronics & Materials Science Directorate	1
NASA Headquarters Washington, DC 20546 ATTN: Code RN	1
Naval Surface Warfare Center Port Hueneme Division 4363 Missile Way Port Hueneme, CA 93043-4307 ATTN: Library	1
Metals Information Analysis Center Purdue University 2595 Yeager Road West Lafayette, IN 47906-1398	1
Office of Naval Research European Office PSC 802 Box 39 FPO AE 09499-0700	1
National Institute of Standards and Technology Gaithersburg, MD 20899 ATTN: Metallurgy Division	1
Naval Facilities Engineering Command 200 Stoval Street Alexandria, VA 22332-2300 ATTN: Code 15R	1
Oak Ridge National Laboratory Metals and Ceramics Div. P.O. Box X Oak Ridge, TN 37380	1
Los Alamos Scientific Lab. P.O. Box 1663 Los Alamos, NM 87544 ATTN: Report Librarian	1
Argonne National Laboratory Metallurgy Division P.O. Box 229 Lemont, IL 60439	1
Brookhaven National Laboratory Upton, Long Island, NY 11973 ATTN: Research Library	1
Lawrence Berkeley Lab. 1 Cyclotron Rd. Berkeley, CA 94720 ATTN: Library	1
Office of Naval Research Asian Office Unit 45002 APO Area Pacific 96337-0007	1

May 1997

Supplemental Distribution List
Technical Reports and Publications

Dr. Paul Pemsler
Castle Technology
P.O. Box 5
Lexington, MA 02173-0005

Profs. G.H. Meier and F.S. Pettit
Dept. of Mat'ls Science & Eng.
848 Benedum Hall
University of Pittsburgh
Pittsburgh, PA 15261

Prof. Gordon P. Bierwagen
North Dakota State University
Dept. of Polymers and Coatings
Box 5227
Fargo, ND 58105

Prof. H.W. Pickering
The Pennsylvania State University
209 Steidle Bldg.
University Park, PA 16802

Prof. D.J. Duquette
Dept. of Metallurgical Eng.
Rensselaer Polytechnic Inst.
Troy, NY 12181

Dr. Robert Clarke
Naval Surface Warfare Center
Carderock Division
Bldg. 60 Code 613
9500 McArthur Blvd.
West Bethesda, MD 20817-5700

Dr. Linn W. Hobbs
Massachusetts Institute of
Technology
Dept. of Materials Science &
Engineering
Cambridge, MA 02139-4307

Mr. E. D. Thomas
Code 6310
Naval Research Laboratory
4555 Overlook Ave., S.W.
Washington, DC 20375-5320

Dr. D.D. MacDonald
The Pennsylvania State Univ.
517 Deike Bldg.
University Park, PA 16802

Dr. B. G. Pound
SRI International .
333 Ravenswood Ave.
Menlo Park, CA 94025

Mr. Robert J. Ferrara
Naval Surface Warfare Center
Carderock Division
Bldg. 60 Code 613
9500 McArthur Blvd.
West Bethesda, MD 20817-5700

Dr. Anthony Eng
Naval Air Warfare Center
Aircraft Division
Code 434, Mail Stop 3 Bldg. 2188
48066 Shaw Rd.
Patuxent River, MD 20670-5304

Supplemental Distribution List
Technical Reports and Publications

Dr. M. W. Kendig
Rockwell International Sci. Ctr.
1049 Camino Dos Rios
P.O. Box 1085
Thousand Oaks, CA 91360

Dr. Jean Montemarano
Naval Surface Warfare Center
Carderock Division
Bldg. 60 Code 641
9500 McArthur Blvd.
West Bethesda, MD 20817-5700

Dr. P.S. Pao
Code 6310
Naval Research Laboratory
4555 Overlook Ave., S.W.
Washington, D.C. 20375-5320

Dr. W.P. Allen
United Technologies Research Center
East Hartford, CT 06108

Dr. B. A. Shaw
Dept. of Eng. Sci. & Mechanics
211 Hallowell Building
The Pennsylvania State University
University Park, PA 16802-6804

Dr. P. Cox
SRI International
333 Ravenswood Ave.
Menlo Park, CA 94025-3493

Dr. Clyde L. Briant
Division of Engineering
Brown University
Providence, RI 02912

Prof. K. Sieradzki
Dept. of Mechanical & Aerospace Eng.
Arizona State University
Box 876106
Tempe, AZ 85287-6106

Dr. John Murray
Naval Surface Warfare Center
Carderock Division
Bldg. 60 Code 613
9500 McArthur Blvd.
West Bethesda, MD 20817-5700

Dr. Laura J. Turbini
Georgia Institute of Technology
Materials Science and Engineering
778 Atlantic Drive
Atlantic, GA 30332-0245

Prof. M.E. Orazem
Dept. of Chemical Engineering
University of Florida
Gainesville, FL 32611

Dr. Patricia Trzaskoma-Paulette
Code 6310
Naval Research Laboratory
4555 Overlook Ave., S.W.
Washington, D.C. 20375-5320

Prof. R. C. Newman
UMIST
Corrosion and Protection Center
P.O. Box 88
Manchester M60 1QD, U.K.

Prof. S.C. Dexter
College of Marine Studies
University of Delaware
700 Pilottown Rd.
Lewes, DE 19958